JCTC Journal of Chemical Theory and Computation

Chemically Meaningful Atomic Charges That Reproduce the Electrostatic Potential in Periodic and Nonperiodic Materials

Thomas A. Manz* and David S. Sholl*

School of Chemical and Biomolecular Engineering, Georgia Institute of Technology, Atlanta, Georgia 30332-0100

Received March 5, 2010

Abstract: Net atomic charges (NACs) can be used both to understand the chemical states of atoms in a material as well as to represent the electrostatic potential, *V*, of the material outside its electron distribution. However, many existing definitions of NACs have limitations that prevent them from adequately fulfilling this dual purpose. Some charge methods are not applicable to periodic materials or are inaccurate for systems containing buried atoms, while others work for both periodic and nonperiodic materials containing buried atoms but give NACS that do not accurately reproduce *V*. We present a new approach, density derived electrostatic and chemical (DDEC) charges, that overcomes these limitations by simultaneously optimizing the NACs to be chemically meaningful and to reproduce *V* outside the electron distribution. This atoms-in-molecule method partitions the total electron density among atoms and uses a distributed multipole expansion to formally reproduce *V* exactly outside the electron distribution. We compare different methods for computing NACs for a broad range of materials that are periodic in zero, one, two, and three dimensions. The DDEC method consistently performs well for systems with and without buried atoms, including molecules, nonporous solids, solid surfaces, and porous solids like metal organic frameworks.

Introduction

The electron density in a material, $\rho(\vec{r})$, controls almost all fundamental properties of the material. In many contexts, however, it is useful to replace this complicated function by the simpler concept of a single charge associated with each of the material's atoms. Atomistic simulations based on interatomic force fields, which provide a crucial tool in the multiscale modeling of complex materials,[1] often rely on charges of this kind for their definition. Atomic charges also provide a simple approach for characterizing charge transfer and similar properties. The task of assigning net atomic charges (NACs) to individual atoms from $\rho(\vec{r})$ obtained from a quantum chemistry calculation is a long-standing challenge that has no unique solution.[2] To be widely applicable, an approach to this task should satisfy several criteria. First, the method should be directly applicable to both periodic and nonperiodic systems; specifically, the method should not require the use of a nonperiodic cluster to assign charges for periodic materials. Second, to accurately describe electrostatic interactions between chemical species, the NACs should accurately reproduce the electrostatic potential, *V*, outside the electron distribution. Third, to be chemically meaningful, the assigned atomic distributions and NACs should resemble those of real atoms in appropriate reference states. Fourth, the method should be applicable to both porous and nonporous materials. Finally, the method should yield a well-defined set of NACs that are independent of the basis sets used to generate the electron density.

Common methods for computing NACs fail to satisfy one or more of the criteria above. Electrostatic potential (ESP) fitting methods assign NACs that minimize the RMS deviation in *V* over a set of grid points outside the van der Waals (vdW) surface of a material relative to *V* from the full electron density.[3,4] In systems containing buried atoms, many different combinations of charges on atoms far from

* E-mail: thomasamanz@gmail.com (T.A.M.), david.sholl@chbe.gatech.edu (D.S.S.).

10.1021/ct100125x
Published on Web 07/15/2010

the vdW surface can give almost the same V, giving ESP charges that are not chemically meaningful.[5] (An atom is buried if its minimum distance to the system's vdW surface is larger than the atom's vdW radius.) For large molecules, this problem can be addressed,[3,6] but for spatially extended materials, ESP charges are typically obtained from nonperiodic cluster models, where it is not straightforward to determine the optimal cluster size or truncation.[7] The recent REPEAT method overcomes these problems, allowing NACs to be fit to V in porous periodic materials without constructing a nonperiodic cluster model, but it has only limited applicability to nonporous solids.[8] The Hirshfeld (HD) method[9] is applicable to both periodic and nonperiodic systems but underestimates the magnitudes of NACs.[10,11] The recent iterative stockholder atom (ISA) and iterative Hirshfeld (IH) methods reproduce V and molecular dipoles,[10,12−16] but they have not yet been applied to compute NACs in periodic materials. An alternative widely applied to periodic systems is the Bader decomposition, which associates the electron density in cleverly constructed volumes to each atom.[17,18] Bader NACs are chemically meaningful and suitable for materials containing buried atoms, but they do not accurately reproduce V outside the electron distribution. The well-known Mulliken method has the key drawback of explicit basis set dependence.[19] Natural population analysis (NPA) solves this basis set problem,[19] but NPA is not readily available for periodic systems. This brief review indicates that no approach is currently available that meets all of the criteria listed above.

Below, we introduce a new approach, density derived electrostatic and chemical (DDEC) charges, to associating charges with atoms from a known electron density. DDEC charges satisfy all of the criteria defined above. We present results for materials that are periodic in zero, one, two, and three dimensions, for dense solids, for porous solids, for surfaces of solids, for small molecules, and for large molecules with buried atoms. These examples include many different chemical elements, emphasizing the broad applicability of the method. In each example, we compare the performance of the DDEC method to several existing charge calculation methods. The DDEC method is among the best performing methods for each system, and none of the other charge methods we tested were as accurate as DDEC for such a wide range of systems. The ESP (REPEAT) method is the most accurate for fitting V in nonperiodic (periodic) materials without buried atoms but requires the addition of fine-tuned constraints to accurately treat systems with buried atoms.[3,6,8] The DDEC method does not require such constraints to compute accurate charges in systems with buried atoms. We also find that the DDEC NACs exhibit good transferability between related chemical systems. These properties make the DDEC NACs well-suited for the construction of force fields used in atomistic simulations and for the interpretation of charge transfer during chemical reactions.

Theory

We begin by defining an arbitrary material as a set of atoms $\{A\}$ at positions $\{\vec{R}_A\}$, in a reference unit cell, **U**. For a nonperiodic system (e.g., a molecule), **U** is any parallelpiped enclosing the entire electron distribution. The total electrostatic potential, V, can be written as a sum of atomic electrostatic potentials:

$$V(\vec{r}) = \sum_{k_1} \sum_{k_2} \sum_{k_3} \sum_{A} V_A(\vec{r}_A) \quad (1)$$

Here, the reference unit cell has $k_1 = k_2 = k_3 = 0$ and summation over A means summation over all atoms in this unit cell. For a periodic direction, k_i ranges over all integers with the associated lattice vector $\vec{v}_i$. For a nonperiodic direction, $k_i = 0$ and $\vec{v}_i$ is the corresponding edge of **U**. In this sum

$$\vec{r}_A = \vec{r} - k_1\vec{v}_1 - k_2\vec{v}_2 - k_3\vec{v}_3 - \vec{R}_A \quad (2)$$

where $V_A(\vec{r}_A)$ is defined as the electrostatic potential due to the charge assigned to atom A

$$V_A(\vec{r}_A) = \frac{z_A}{r_A} - \oint \frac{\rho_A(\vec{r}'_A)\, d^3\vec{r}'_A}{|\vec{r}_A - \vec{r}'_A|} = \frac{q_A}{r_A} + B + C \quad (3)$$

where $\rho_A(\vec{r}_A)$ is the non-negative electron density assigned to atom A, z_A is the nuclear charge, q_A is the NAC, and $r_A = |\vec{r}_A|$. Since $V_A(\vec{r}_A)$ outside the charge distribution can be exactly represented by a multipole expansion,[20,21] we can rewrite $V_A(\vec{r}_A)$ as shown on the right-hand side of eq 3 where B and C are terms due to atomic multipoles (AMs) and penetration of the atom's electron density, respectively. AMs can be computed by applying the method of Laidig[21] or Kosov and Popelier[20] to $\rho_A(\vec{r}_A)$. The penetration term, C, decays approximately exponentially with increasing r_A and is essentially zero for r_A greater than a critical radius where ρ_A becomes negligible.[22] As in other atoms-in-molecule (AIM) methods,[9,10,14,17,23] we impose the constraint that the entire electron density is included in the collection of atomic densities, which requires $\Theta(\vec{r}) = 0$ where

$$\Theta(\vec{r}) = \rho(\vec{r}) - \sum_{k_1} \sum_{k_2} \sum_{k_3} \sum_{A} \rho_A(\vec{r}_A) \quad (4)$$

To be chemically meaningful, NACs should indicate the amount of charge transfer between atoms. Imagine building a chemical system from isolated atoms in a thought experiment. Noninteracting atoms are first placed at the appropriate atomic positions. The choice of noninteracting atoms for this prematerial is not unique: for NaCl, we could choose either neutral Na and neutral Cl or Na^+ and Cl^-. Because there is no charge transfer between the atoms yet, the computed NACs for this noninteracting prematerial should equal the isolated atom charges. The IH and ISA methods satisfy this prematerial charge criterion,[13] but the Bader method does not.[24] The HD method only satisfies this criterion if the prematerial atoms are neutral, but this is not possible for systems containing a net charge. When the interactions between atoms are included, charges are transferred between them to form the real system. We now show how an AIM method can be developed that simultaneously accounts for the different types of charge transfer in interacting systems.

For ionic charge transfer, the density of each atom in the interacting system, $\rho_A(\vec{r}_A)$, should approximately equal the density of that atom in a noninteracting reference state, $\rho_A^{ref}(r_A,n_A)$, having the same number of electrons, n_A. To achieve this, we minimize a distance measure between $\rho_A(\vec{r}_A)$ and $\rho_A^{ref}(r_A,n_A)$ subject to the constraint $\Theta(\vec{r}) = 0$. The IH method involves a suitable distance measure of this type:[10]

$$F_{chem} = \sum_A \oint \rho_A(\vec{r}_A) \ln\left(\frac{\rho_A(\vec{r}_A)}{\rho_A^{ref}(r_A,n_A)}\right) d^3\vec{r}_A \quad (5)$$

Setting $\partial F_{chem}/\partial\rho_A(\vec{r}_A) = 0$ leads to a proportional distribution of electrons between atoms, $\rho_A(\vec{r}_A)/\rho_A^{ref}(r_A,n_A) = \rho_B(\vec{r}_B)/\rho_B^{ref}(r_B,n_B)$, which is a type of Stockholder partitioning.[15] The reference state density is the linear interpolation

$$\rho_A^{ref}(r_A,n_A) = (1-f)\rho_A^{\tau}(r_A) + f\rho_A^{\tau+1}(r_A) \quad (6)$$

between the spherically averaged ground state densities of isolated atoms of the same element having the closest lower (τ) and higher ($\tau + 1$) integer number of electrons, where $f = n_A - \text{floor}(n_A) = n_A - \tau$.[10,12,13] Instead of being based on single atoms, the reference states could be based on chemical fragments containing several atoms, which would give fragment net charges rather than NACs. A modification of this type to the IH method has been used to study charge transfer between a graphene sheet and adsorbates.[25]

The second type of charge transfer is covalent bonding. This type of charge transfer is directional in nature and generates nonspherical distortions in the electron density of each atom. Multipole contributions sum to zero for spherically symmetric distributions, so eq 1 converges most rapidly if each $\rho_A(\vec{r}_A)$ is optimized to be as close to spherically symmetric as possible. Since a key objective is to compute NACs that accurately reproduce V outside the electron distribution, the atomic distributions should be optimized to be close to spherically symmetric. In the ISA method,[13−15] this is done by minimizing the information distance, F_{ESP}, between $\rho_A(\vec{r}_A)$ and its spherical average, $\rho_A^{avg}(r_A)$, subject to the constraint $\Theta(\vec{r}) = 0$, where

$$F_{ESP} = \sum_A \oint \rho_A(\vec{r}_A) \ln\left(\frac{\rho_A(\vec{r}_A)}{\rho_A^{avg}(r_A)}\right) d^3\vec{r}_A \quad (7)$$

Setting $\partial F_{ESP}/\partial\rho_A(\vec{r}_A) = 0$ gives $\rho_A(\vec{r}_A)/\rho_A^{avg}(r_A) = \rho_B(\vec{r}_B)/\rho_B^{avg}(r_B)$, which is a type of Stockholder partitioning where density is given to each atom in proportion to $\rho_A^{avg}(r_A)$. The effects on V of slight deviations of $\rho_A(\vec{r}_A)$ from spherical symmetry are accounted for by the AMs of $\rho_A(\vec{r}_A)$. Because AM contributions are minimized by making $\rho_A(\vec{r}_A)$ close to spherically symmetric, the ISA NACs are often very similar to those obtained with the ESP method.

The third type of charge transfer is a response to overall changes in the electric field. For example, the electron density of an isolated O^{2-} ion in a vacuum decays very slowly with increasing radius because of strong repulsion between the excess valence electrons. A crystal containing O^{2-} ions contains cations that provide charge compensation, and the dielectric constant of the crystal is larger than that of the vacuum. Charge compensation and dielectric screening reduce the strength of electrostatic repulsion between valence electrons in an O^{2-} ion, causing it to have a smaller effective radius in a crystal than in a vacuum. As shown in the Results and Discussion section below, the use of uncompensated reference states (i.e., vacuum phase ions) to construct $\rho_A^{ref}(r_A,n_A)$ leads to chemically unreasonable NACs in many cases, for example, charge magnitudes significantly greater than 2 in crystalline MgO. To solve this problem, charge-compensated ions should be used to construct $\rho_A^{ref}(r_A,n_A)$. One possible approach is to place all of the compensating charge on the surface of an atom-centered sphere having a radius chosen to approximately coincide with the anionic radius,[26] such as has been used in the interpretation of experimental electron density profiles for MgO and other ionic solids.[27] Our modification of this approach allows the anionic radius to be determined self-consistently by energy minimization. For cations, we developed a different approach involving a spherical charge compensation shell. As a conceptually simpler alternative, we also developed a periodic charge compensation scheme for both anions and cations that employs a uniform background charge. Details of these approaches are described in the Methods section below.

Table 1. Optimization of the Parameter χ

	h-BN crystal			BN sheet		
χ	iterations	AM_{max}	q_B	iterations	AM_{max}	q_B
0.00	422	0.27(q)	0.64	1550	0.11(q)	1.07
0.05	243	0.21(q)	1.00	171	0.16(q)	1.04
0.10	149	0.24(q)	0.96	142	0.23(q)	0.99
0.20	90	0.32(q)	0.90	86	0.36(q)	0.91
0.50	47	0.58(q)	0.79	46	0.66(q)	0.79
1.00	29	0.92(q)	0.70	28	1.03(q)	0.69

When all atoms are near the surface of a material, only one set of NACs approximately reproduces V. Because the ISA NACs are optimized to reproduce V, the optimization landscape for F_{ESP} is likewise steep when the system contains no buried atoms. In this case, the ideal force field NACs are those which approximately minimize F_{ESP} irrespective of F_{chem} and correspond to the well-determined ESP charges. For systems containing buried atoms, multiple sets of NACs can reproduce V with similar accuracy. Including F_{chem} in the optimization functional will ensure that the optimized NACs are chemically meaningful, because the atomic distributions are optimized to resemble those of real atoms in appropriate reference states. Thus, we propose an optimization functional of the form

$$G = \chi F_{chem} + (1-\chi)F_{ESP} + \int_U \lambda(\vec{r})\,\Theta(\vec{r})\,d^3\vec{r} \quad (8)$$

to conveniently handle systems with and without buried atoms, where the Lagrange multiplier $\lambda(\vec{r})$ enforces the constraint $\Theta(\vec{r}) = 0$. F_{chem} and F_{ESP} should be weighted non-negatively, so $0 \le \chi \le 1$. For optimum performance, F_{chem} should be weighted much less than F_{ESP} so that F_{chem} only becomes important when F_{ESP} defines a shallow landscape (i.e., for systems containing buried atoms); thus, $0.01 \le \chi \le 0.4$. Table 1 shows the effects of changing χ on the charges and largest atomic multipole (AM_{max}) for a single sheet of

hexagonal BN and the three-dimensional solid form of h-BN formed by stacking these sheets (see Figure 1). Computational details are provided in the Methods section below. Since the sheets in h-BN are weakly bound to each other, an ideal charge method should give similar NACs for these two structures. When no reference density was used (i.e., $\chi = 0$), significantly different charges were obtained for these two structures, illustrating the poor transferability of the ISA method for systems with buried atoms. This problem was solved by including a reference density (i.e., $\chi > 0$), leading to similar charges for the two structures. (C1 charge compensated densities, defined in detail below, were used in this example.) The number of iterations required for convergence decreased monotonically as χ increased from 0 to 1. For h-BN, AM_{max} went through a minimum around $\chi = 0.05$. As described above, small AMs are desirable for the NACs to accurately reproduce V. In the following results, we used $\chi = 0.10$, which provided small AMs at reasonable computational cost. Our approach also makes it possible for the first time to compute ISA and IH NACs for spatially periodic materials, where ISA corresponds to $\chi = 0$ and IH corresponds to $\chi = 1$ using reference ions placed in a vacuum without charge compensation.

Charges are calculated using an iterative scheme. Setting $\partial G/\partial \rho_A(\vec{r}_A) = 0$ for constant $\rho_A^{ref}(r_A,n_A)$ gives

$$\frac{\partial G}{\partial \rho_A(\vec{r}_A)} = (1-\chi)\ln\left(\frac{\rho_A(\vec{r}_A)}{\rho_A^{avg}(r_A)}\right) + \chi \ln\left(\frac{\rho_A(\vec{r}_A)}{\rho_A^{ref}(r_A,n_A)}\right) + \chi - \lambda(\vec{r}) \quad (9)$$

Exponentiating eq 9 gives

$$e^{\lambda(\vec{r})-\chi} = \frac{\rho_A(\vec{r}_A)}{w_A(r_A)} = \frac{\rho_B(\vec{r}_B)}{w_B(r_B)} \quad (10)$$

where the relative weight factor for each atom is

$$w_A(r_A) = (\rho_A^{avg}(r_A))^{(1-\chi)}(\rho_A^{ref}(r_A,n_A))^{\chi} \quad (11)$$

Equation 10 can be more conveniently written by summing over B to give

$$\rho_A(\vec{r}_A) = w_A(r_A)\,\rho(\vec{r})/\sum_{k_1}\sum_{k_2}\sum_{k_3}\sum_{B} w_B(r_B) \quad (12)$$

Neutral atom densities, $\rho_A^{ref}(r_A,0)$, are used as initial estimates. In each iteration, the current estimate of $\{w_A(r_A)\}$ is used to compute $\{\rho_A(\vec{r}_A)\}$ by eq 12. After calculating

$$n_A = \oint \rho_A(\vec{r}_A)\, d^3\vec{r}_A = z_A - q_A \quad (13)$$

the new reference density $\rho_A^{ref}(r_A,n_A)$ is computed via eq 6. Finally, $\rho_A^{ref}(r_A,n_A)$ and the spherical average of $\rho_A(\vec{r}_A)$ are combined using eq 11 to generate an improved estimate of $\{w_A(r_A)\}$. The process is repeated until the NACs for consecutive iterations differ by less than a chosen tolerance. Since neutral atom densities are used for the initial guess, the initial iteration of this scheme gives the HD NACs. (The value of χ does not affect the HD NACs because χ first enters the calculation after the initial iteration is completed.) Because no charge compensation is involved for neutral atoms, the compensated and uncompensated reference density sets give the same HD NACs. Depending on the choice of χ and reference densities, the converged results give the DDEC, ISA, or IH NACs.

Methods

Except where otherwise noted, density functional theory (DFT) with the PW91 exchange-correlation functional was used to obtain $\rho(\vec{r})$. The PBE functional was used for the iron oxides introduced below. All periodic DFT calculations were performed in the Vienna Ab Initio Simulation Package[28,29] (VASP) using the projector augmented wave (PAW) method[30] and a 400 eV cutoff. For periodic systems, the product of the number of k points and the unit cell volume exceeded 4000 Å^3. Except where otherwise noted, nonperiodic DFT calculations were performed using Gaussian software[31] with 6-311++G** basis sets. LANL2DZ basis sets and the B3LYP functional were used for the Zr complexes introduced below. DDEC charges should be computed using an all-electron density. PAW is a frozen-core method that yields all-electron densities. Since LANL2DZ employs an effective core potential (ECP) for the 28 innermost electrons of Zr, we added the PAW frozen-core distribution of these 28 electrons to the LANL2DZ-derived SCF electron density to obtain the all-electron density of each Zr complex, which was then used to compute the DDEC charges. The PAW and ECP methods treat the core electrons relativistically, which is important for modeling heavy atoms. Experimental structures were used for MIL-53 (Al),[32] h-BN,[33] and IRMOF-1,[34] while all other geometries were optimized. Bader charges were computed using the software developed by Henkelman and co-workers.[35−37]

Electrostatic potentials in the periodic systems were computed using the Ewald summation of Smith that includes point charges and optionally point dipoles or quadrupoles.[38] Enough terms were included in the real and reciprocal space sums to converge $V(\vec{r})$ to better than 0.06 kcal/mol. In the

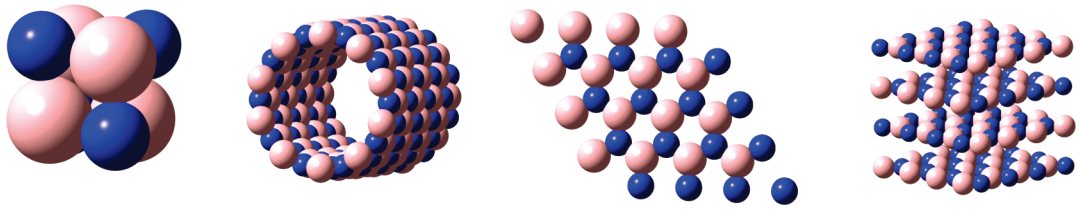

Figure 1. BN structures used in Table 2. From left to right: B_4N_4 cluster, (10,10) nanotube, hexagonal sheet, and hexagonal crystal (h-BN).

results below, ΔV_{NAC} is the RMS difference between the ab initio $V(\vec{r})$ and the potential due to the NACs. ΔV_{dip} is similarly defined, except it includes the potential due to both the NACs and the atomic dipoles. The grid points used to compute ΔV_{NAC} and ΔV_{dip} were uniformly distributed between the surfaces defined by 1.4× and 2.0× vdW radii, which is the region of interest for ESP fitting methods.[4] In periodic systems, V is only determined up to an arbitrary constant,[8] so the average V over these grid points was set equal for the two systems. We used previously reported vdW radii applicable to the first 96 elements.[39]

Since alternative methods can be used to generate charge compensated reference densities, one should include the reference density set label when reporting charges obtained by the DDEC method. In the results below, DDEC/c1 denotes the use of $\chi = 0.1$ with "c1" reference densities computed in VASP by the following method. The ion was placed in the center of a cubic unit cell having an edge length of 10 Å. The cutoff energy, PW91 functional, k-point spacing, and PAW method described in the first paragraph of this section were used. The total number of electrons, n_A, was specified to give the desired ion charge. The energy and electron density were then converged to give the spin state with the lowest energy. During this DFT calculation, the unit cell is made neutral by adding a uniform background charge. This uniform background charge provides charge compensation and only affects the electron density by modifying the net electric field. Moreover, the periodic array of atoms provides dielectric screening that further reduces the electric field strength. This simulates the charge compensation and dielectric screening that occurs in real materials, thereby providing more accurate reference densities than would be obtained from uncompensated ions. For comparison, we also performed charge analysis using uncompensated vacuum reference ions. In the results below, uncompensated (UC) denotes the use of $\chi = 0.1$ with reference densities computed in Gaussian using the PW91 functional and 6-311++G** basis sets (LANL2DZ on Zr and WTBS on Sr).

DDEC/c2 denotes the use of $\chi = 0.1$ with "c2" reference densities computed using a spherical surface of compensating charge having radius R_{comp}. Through trial and error, we found that a careful choice of R_{comp} is required to obtain accurate NACs. No compensating charge was used for the neutral atoms. Let q_1 be the net charge (including the nuclear charge) closer to the atomic center than R_{comp}, q_2 the compensating charge at R_{comp}, and $q_3 < 0$ the net charge due to electron density farther from the nucleus than R_{comp}. Since $q_3 < 0$, making the overall system neutral (i.e., $q_1 + q_2 + q_3 = 0$) gives $q_1 + q_2 > 0$, which produces a cation-like behavior for the spherical ball including R_{comp}. Thus, for cations, the surface charge q_2 was constrained to make the overall system neutral. Since $q_3 < 0$, for $q_1 + q_2 = 0$ the net charge enclosed in a ball of radius $r > R_{comp}$ is slightly negative, and this causes a weak Coulombic repulsion of electrons from the nucleus for $r > R_{comp}$. Because this is the correct behavior for a compensated anion, we infer that $q_1 + q_2 = 0$ is a suitable constraint for anions. By Gauss's law, the constraint $q_1 + q_2 = 0$ can be imposed by choosing a surface charge distribution that makes the electric field zero infinitesimally outside R_{comp}. For anions, R_{comp} was iteratively adjusted by increments of 0.05 Å until the system's total energy was minimized. Values of R_{comp} determined in this manner are similar to crystal-structure-derived anionic radii reported in the CRC Handbook of Chemistry and Physics; specifically, R_{comp} (crystal-structure-derived anionic radii[40]) values in Å are 1.25 (1.33) for F^-, 1.80 (1.81) for Cl^-, 1.95 (1.96) for Br^-, 2.20 (2.20) for I^-, 1.30 (1.21−1.42) for O^{2-}, 1.80 (1.84) for S^{2-}, 1.95 (1.98) for Se^{2-}, and 2.20 (2.21) for Te^{2-}.

For a cation, R_{comp} should be chosen so electrons are attracted less strongly to the nucleus than in the uncompensated cation, but more strongly than in the neutral atom. The following procedure ensures this. First, consider the mth moment of the radius

$$\langle r_i^{(m)} \rangle = \oint r^m \phi_i^*(\vec{r})\, \phi_i(\vec{r})\, d^3\vec{r} \qquad (14)$$

for each occupied Kohn−Sham spin−orbital in the neutral atom. Because the spin−orbital is normalized, the moment for $m = 0$ is 1, while $\langle r_i^{(1)} \rangle$ gives the average radius of the spin−orbital. $\langle r_i^{(-1)} \rangle$ is the average electrostatic potential magnitude exerted by the spin−orbital on the center of the nucleus. Because $m = 1$ weights points in proportion to r while $m = -1$ weights points in proportion to $1/r$, the average potential magnitude exerted on the nucleus is greater than if the electron's entire charge were placed at the average radius:

$$\langle r_i^{(-1)} \rangle > \langle r_i^{(1)} \rangle^{-1} \qquad (15)$$

Accordingly, if we choose R_{comp} as the average of the q largest $\langle r_i^{(1)} \rangle$ chosen from the z_A occupied spin−orbitals of the neutral atom, then the electrostatic potential magnitude exerted by the compensating charge on the nucleus will necessarily be less than for any q electron spin−orbitals present in the neutral atom but greater than if no compensating charge is used. This procedure was used to compute the R_{comp} of the cations, because it gives compensation in the required range between that of the neutral atom and the uncompensated $+q$ cation.

Close examination shows that the conductor-like polarizable continuum model (CPCM) and the c2 compensation method have the same mathematical form when the cavity radius in the CPCM model is set equal to R_{comp}. When no further constraints are added, the CPCM model chooses a polarization charge distribution to make the electric field zero infinitesimally outside the cavity wall, which is the appropriate constraint for c2 anions. The wave function and polarization charge distribution are determined self-consistently with each affecting the other. Analogous to the Hartree−Fock method in which the electron−electron potential operator is twice the electron−electron energy operator, the unconstrained CPCM potential operator is twice the CPCM energy operator.[41] The Gaussian output file lists the polarization charge, q_{CPCM}, corresponding to the potential operator, so $q_{CPCM} = 2q_2$ for anions. For example, direct integration of the enclosed charge for the c2 O^{2-} ion gave $q_1 = -0.865$, while the Gaussian output gave a polarization charge of $q_{CPCM} = 1.735$, which is within an integration tolerance of $2q_2 = -2 \times q_1 = 1.73$. For cations, q_{CPCM} is constrained (using

the Gaussian keyword IComp=1) to give a net charge of zero (i.e., $q_1 + q_{CPCM} + q_3 = 0$), which gives $q_{CPCM} = q_2$ for cations. In this case, q_{CPCM} has a constant value independent of the wave function so it behaves as an external potential with equal energy and potential operators. For the c2 Mg^{2+} ion, the Gaussian output listed a polarization charge of $q_{CPCM} = -1.998$ which is within an integration tolerance of $q_2 = -2$. The c2 reference densities were computed in Gaussian 09 using the CPCM smoothing method of York and Karplus.[41] Example input files are given in the Supporting Information. To ensure applicability to all elements of the periodic table, a universal Gaussian basis set (UGBS) based on the work of de Castro and Jorge[42] was used, and relativistic corrections were included using the fourth order Douglas−Kroll−Hess method with spin−orbit coupling and a finite nuclear model. In this UGBS, we used the same exponents and same spdf shells for all elements, giving 294 basis functions per atom. Having two different charge compensation methods (c1 and c2) makes it easier to compute a complete set of reference densities for the chemical elements by providing options in cases where convergence of one method is more difficult than the other. Because they do not involve periodic boundary conditions, the c2 reference densities converged more readily than the c1 reference densities and decayed exponentially with increasing radius.

Our code implementing the DDEC method is freely available from ddec.sourceforge.net. Our results were computed with this code as follows. Valence and core electron densities were output from VASP or Gaussian on a grid of $N_1 \times N_2 \times N_3$ points defined by translation vectors $\vec{v}_1/N_1$, $\vec{v}_2/N_2$, and $\vec{v}_3/N_3$. We chose density grids such that the summed valence density gave the exact number of valence electrons, n_{val}, to within the greater of 0.1 electrons or 0.03%, then normalized the valence density from the grid to give n_{val}. To ensure integration accuracy, our code did not allow any single grid point to contribute more than 0.03 valence electrons. The code ensured that the electron density of each grid point was not negative and used a zero tolerance to avoid division by zero in eqs 5, 7−12. ${\rho_A}^{\tau}(r_A)$ and ${\rho_A}^{avg}(r_A)$ were computed on 50 radial shells equally spaced between $r_A = 0$ and 3.0 Å. NACs were considered converged when successive iterations resulted in a change of less than 5×10^{-5} e for each atom. Upon convergence, the code generates AMs up to quadrupole order. We performed the following tests for MgO and NaF solids to ensure the accuracy of these integration parameters: (a) doubling N_1, N_2, and N_3 changed the DDEC/c1 (c2) cation charge by −0.006 (−0.007) e for MgO and −0.0002 (−0.0003) e for NaF and (b) using 100 radial shells equally spaced between $r_A = 0$ and 5.0 Å changed the DDEC/c1 (c2) cation charge by +0.042 (+0.002) e for MgO and +0.009 (+0.015) e for NaF.

To improve integration accuracy and reduce computational expense, we treat valence and core electron densities separately. Since $\rho(\vec{r})$ has a cusp near each nucleus, an extremely fine grid spacing would be required to accurately integrate ${\rho_A}^{core}(\vec{r}_A)$. We avoided this problem by using the (integer) number of core electrons, ${n_A}^{core}$, obtained from chemical knowledge. For each atom, the number of valence electrons, ${n_A}^{val}$, is obtained by integrating

$$\rho_A^{val}(\vec{r}_A) = \rho_A(\vec{r}_A) - \rho_A^{core}(\vec{r}_A) \quad (16)$$

which is used to compute ${n_A} = {n_A}^{core} + {n_A}^{val}$. ${\rho_A}^{core}(\vec{r}_A)$ is found by performing an ISA analysis on $\rho^{core}(\vec{r})$, which is accurate because core electron distributions for different atoms are spherically symmetric and barely overlap. Previous implementations of the IH and ISA methods did not use valence-core separation (VCS).[10,12−16] To validate this approach, NACs for h-BN and formamide were computed using the HD, IH, ISA, DDEC/c1, and UC methods. For each method, the RMS difference in NACs computed with and without VCS was only 0.01e, except that IH gave a RMS difference of 0.03e. Not using VCS led to a change in the DDEC/c1 (c2) cation charge of −0.007 (−0.007) e for MgO and +0.018 (+0.030) e for NaF solids relative to NACs computed with VCS. VCS is critical for calculating NACs in large systems, where a fine grid would be too computationally expensive. Using VCS, the DDEC and IH NACs for IRMOF-1, which contains 424 atoms in the unit cell, were computed in much less time than was required for the DFT calculation to generate the electron density. ISA took substantially more iterations and time to converge than DDEC and IH.

Results and Discussion

We now turn to a series of examples that illustrate the properties of DDEC charges and their advantages relative to other charge partitioning methods. In all of the results below, atomic charges and multipoles are given in Hartree atomic units, which use 1e and Bohr as the unit charge and length, respectively. All ΔV_{NAC} and ΔV_{dip} values are in kcal/mol for a test charge of 1e. AM_{max} denotes the largest atomic dipole magnitude (labeled d) or quadrupole component (labeled q) in atomic units. The dominant quadrupole component was

$$Q_{3z^2-r^2} = -\oint (3(\vec{r}_A \cdot \hat{z})^2 - r_A^2)\rho_A(\vec{r}_A)\, d^3\vec{r}_A \quad (17)$$

The z direction was perpendicular to the plane containing the formamide atoms, the BN sheet, the hexagonal planes in h-BN, and the BN nanotube axis.

To highlight the applicability of DDEC charges to both clusters and extended materials, we first examined the zero-, one-, two-, and three-dimensional BN structures shown in Figure 1. The atomic charges computed with a variety of AIM methods are summarized in Table 2, where it is clear that the choice of AIM method has a large effect on the computed NAC. For the 3D crystal, for example, q_B varied from 0.19 (HD) to 2.13 (Bader) with ISA, IH, DDEC, and UC giving intermediate values. Table 2 also includes information about the atomic multipoles (AMs) for each BN material. Including F_{ESP} in the calculation of atomic charges reduced the magnitudes of the AMs. For the DDEC, ISA, and UC methods, which include F_{ESP}, every atomic dipole and quadrupole component was ≤0.5 for all four materials. Bader, HD, and IH calculations, which do not include F_{ESP},

Table 2. Charge Analysis for the BN Structures Shown in Figure 1, with AIM Methods Listed in Order of Ability to Reproduce *V*

	B_4N_4 cluster			BN nanotube			BN sheet			h-BN crystal	
	q_B	AM_{max}	ΔV_{NAC}	q_B	AM_{max}	$\Delta V_{NAC}(\Delta V_{dip})$	q_B	AM_{max}	ΔV_{NAC}	q_B	AM_{max}
V-fit	0.78		0.4	0.47		0.89	0.86		0.5		
DDEC/c1	0.79	0.2d	0.6	1.00	0.2q	7.1(3.2)	0.99	0.2q	0.5	0.96	0.2q
DDEC/c2	0.817	0.2d	0.7	1.088	0.3q	8.2(3.7)	1.09	0.4q	0.5	1.07	0.4q
ISA	0.82	0.2d	0.8	1.09	0.1q	8.5(2.4)	1.07	0.1q	0.5	0.64	0.3q
UC	0.84	0.2d	0.9	1.14	0.4q	8.9(4.2)	1.14	0.5q	0.5	1.12	0.5q
IH	0.89	0.5d	1.3	1.12	2.6q	8.6(16.2)	1.10	2.8q	0.5	1.14	2.3q
HD	0.27	0.5q	4.3	0.20	1.8q	3.5(10.7)	0.20	1.8q	0.6	0.19	1.5q
Bader	0.92	0.7d	1.5	2.16	2.4d	21.0	2.13	2.7d	0.9	2.13	1.6d
no charge	0		6.7	0		5.9	0		0.7		

Table 3. Charge Analysis for Several Solid Materials and NaF Slab

	NaF slab q_{Na} for layer				Na F bulk	NaCl bulk	MgO bulk	MgH_2 bulk		$SrTiO_3$ bulk		
	top	2	3	4	q_{Na}	q_{Na}	q_{Mg}	q_{Mg}	q_H	q_{Sr}	q_{Ti}	q_O
Bader	0.82	0.80	0.80	0.80	0.80	0.82	1.71	1.58	−0.79	1.54	1.88	−1.14
DDEC/c1	1.00	1.03	1.02	1.02	1.02	0.97	2.02	1.54	−0.77	1.96	2.48	−1.48
DDEC/c2	1.00	1.00	1.00	1.00	1.00	0.94	2.05	1.62	−0.81	1.99	2.60	−1.53
HD	0.37	0.34	0.35	0.35	0.33	0.27	0.37	0.32	−0.16	0.66	0.45	−0.37
IH	1.05	1.07	1.08	1.09	1.06	1.01	2.23	2.06	−1.03	2.50	3.11	−1.87
ISA	0.94	0.68	0.70	0.62	0.51	0.41	0.63	0.62	−0.31	2.44	−0.22	−0.74
UC	1.01	1.03	1.02	1.02	1.02	0.98	2.13	1.58	−0.79	2.29	2.72	−1.67

had some atomic dipole or quadrupole components ≥ 0.5 for all structures. The overall accuracy of AIM methods for reproducing *V* in these materials was DDEC > ISA > UC > IH > HD > Bader. The c1 and c2 reference densities gave similar results. In agreement with eq 3, methods that minimized AMs were the best overall at reproducing *V*. Charges that minimize ΔV_{NAC} are designated *V*-fit in Table 2. For B_4N_4, these are the ESP charges. For the BN sheet and nanotube, these are the unrestrained REPEAT charges using a uniform grid between the surfaces defined by 1.4× and 2.0× vdW radii. The large difference in *V*-fit charges for the BN sheet ($q_B = 0.86$) and nanotube ($q_B = 0.47$) highlight their poor transferability between similar structures. The standard deviation of AIM charges between the four BN structures followed the trend HD < IH < DDEC < UC < ISA < Bader, which shows that AIM methods including a reference state (HD, IH, DDEC, UC) exhibit the best charge transferability. These results show that the DDEC NACs accurately reproduce *V* with reasonable charge transferability compared to other AIM methods.

To better characterize different AIM methods, it is helpful to use a structure that can be described from chemical knowledge. In crystalline NaF, which is highly ionic, a small spillover of electrons from F^- to Na^+ would lead to $0.6 < q_{Na} \approx 0.9 < 1$, and q_{Na} based on experimental diffraction data is 0.95.[43] For this material, the computed q_{Na}'s were 0.33 (HD), 0.51 (ISA), 0.80 (Bader), 1.00 (DDEC/c2), 1.02 (DDEC/c1 and UC), and 1.06 (IH). The HD charge magnitude was too small because it uses neutral instead of charged reference state atoms.[10] To better understand the ISA result, we examined a NaF(100) surface in a slab calculation of eight layers with the middle four layers fixed at bulk positions, the other layers relaxed, and a vacuum spacing of ~10 Å. As shown in Table 3, q_{Na} for ISA decreased from 0.94 in the surface's top layer to 0.62 in the middle of the slab. This is an example of ISA giving problematic results for a material with buried atoms, an idea supported by the observation that ISA gave reasonable charges for the surface layers. ISA does not constrain the atomic distributions to decay like real atoms as r_A increases. HD, IH, UC, and DDEC do by using a reference density, and the Bader method is an extreme limit where atomic distributions do not overlap. As a result, each of these methods except ISA gave similar NACs for the top and middle layers of the NaF(100) slab.

Charges were also computed for bulk NaCl, $SrTiO_3$, MgO, and MgH_2. Like NaF, q_{Na} for NaCl is expected to be ~0.9. Since $SrTiO_3$ is partially ionic, one expects the NACs to lie between zero and the oxidation states of +2 (Sr), +4 (Ti), and −2 (O). Likewise, the Mg charge is expected to lie between zero and the oxidation state of +2 in MgH_2. The IH and UC NACs did not fall within this range, indicating that these methods are unsuitable for computing NACs in ionic solids. For $SrTiO_3$, the IH (UC) method gave $q_{Sr} = 2.50$ (2.29), which is too large by ~0.50 (~0.29) *e*. The HD and ISA methods failed for the same reasons explained above for the NaF system. The HD charges were too small in magnitude, while the ISA method gave a negative instead of positive charge on Ti in $SrTiO_3$. For all four solids, the Bader method gave NACs less than the oxidation states. The DDEC methods showed that the MgO solid is completely ionic, which agrees with charges extracted from electron diffraction data.[27] The DDEC methods gave reasonable charges, except they often overestimated charge magnitudes by a few hundredths of a unit in completely ionic solids like NaF and MgO. It is hard to pinpoint the source of this small error. Since IH and UC use uncompensated reference densities, while DDEC uses compensated reference densities, these results show the importance of using compensated reference densities when computing charges in solids.

A slab calculation for $SrTiO_3$(100) showed that both DDEC and Bader methods gave chemically reasonable charges for all layers with charges for the middle layers

Table 4. Charge Analysis for Three Oxides Containing Iron in Different Oxidation States

				DDEC c1(c2)			Bader		
	phase	magnetism	Fe oxid. state	q_O	q_{Si}	q_{Fe}	q_O	q_{Si}	q_{Fe}
Fe_2O_3	hematite	antiferro	+3	−1.19 (−1.16)		1.78 (1.74)	−1.05		1.57
Fe_2SiO_4	spinel	antiferro	+2	−1.16 (−1.13)	2.23 (2.21)	1.20 (1.15)	−1.45	3.11	1.34
Fe_3O_4	magnetite	ferri	+3 (tet)	−1.21 (−1.20)		1.76 (1.73)	−1.10		1.46
			+2.5 (oct)			1.54 (1.53)			1.46

converging to the bulk values. This slab was symmetric with a total of four SrO layers and three TiO_2 layers. The geometry of the outer four layers was relaxed, and the inner three layers were fixed at bulk positions. For the top layer, the Sr (O) charges were 1.72 (−1.41) for DDEC/c1, 1.75(−1.46) for DDEC/c2, and 1.61 (−1.26) for Bader, giving a net layer charge of 0.31 (DDEC/c1), 0.29 (DDEC/c2), and 0.35 (Bader). For the next layer, the Ti (O) charges were 2.42 (−1.48) for DDEC/c1, 2.54 (−1.52) for DDEC/c2, and 1.82 (−1.14) for Bader, giving a net layer charge of −0.54 (DDEC/c1), −0.50 (DDEC/c2), and −0.46 (Bader). The subsequent layer charges were similar to the bulk values. Diffraction experiments show that the charge distribution around Sr in bulk $SrTiO_3$ is nearly spherically symmetric, while that between Ti and O is asymmetric; this suggests Sr does not participate in covalent bonding while Ti and O do.[44] Reflections from the spherically symmetric Sr +0 and +2 ions are indistinguishable within the resolution of existing diffraction experiments,[45] making experimental determination of the NACs problematic. Because the DDEC NAC of Sr is approximately an integer (+2) while those of Ti (∼2.5) and O(∼−1.5) are nonintegers, the DDEC results also suggest Sr does not participate in covalent bonding while Ti and O do.

We now consider a series of oxides containing iron in different oxidation states. The oxidation state of Fe in Fe_2SiO_4 is +2, while that in Fe_2O_3 is +3. Magnetite (Fe_3O_4) has an inverse spinel structure containing one Fe +3 oxidation atom in a tetrahedral site and two Fe +2.5 oxidation atoms in octahedral sites. O (Si) have +2 (+4) oxidation states in these compounds. For a given element, a core electron's binding energy measured by X-ray photoelectron spectroscopy (XPS) increases as the net charge or oxidation state of the atom becomes more positive. Yamashita and Hayes measured the Fe $2p_{3/2}$ binding energies as 709.0 ± 0.02 (fayalite phase of Fe_2SiO_4), 710.56 ± 0.05 (magnetite), and 711.0 ± 0.01 (hematite phase of Fe_2O_3) eV, and these binding energies follow the expected trend with increasing average oxidation state.[46] A corresponding trend does not exist for the O 1s binding energies, suggesting no significant differences in the O net charge or oxidation state between these compounds.[46] An unresolved shoulder in the magnetite Fe 3p peak indicates that two different types of Fe are present. Table 4 compares DDEC and Bader charge analysis for Fe_2O_3, Fe_2SiO_4, and Fe_3O_4. For O, the DDEC charges are approximately the same (∼−1.2) in all three materials, while the Bader charge is different (−1.45) for Fe_2SiO_4 than for the other two compounds (∼−1.1). Covalent bonding is suggested since the net charges are much lower in magnitude than the oxidation states. Both the DDEC and Bader methods give higher Fe charge for Fe_2O_3 than for Fe_2SiO_4, which follows the same trend as the Fe oxidation states. For magnetite, DDEC gives a higher net charge for Fe^{tet} than for Fe^{oct}, which follows the expected oxidation state trend and can potentially explain the two different types of Fe observed in the XPS spectrum. The Bader method gives a net charge of 1.46 for both Fe^{tet} and Fe^{oct}.

All of the examples of 3D-periodic materials discussed above were dense materials or surfaces of these solids. As examples of three-dimensional porous materials, we examined two metal−organic frameworks (MOFs). Assigning charges to the atoms in MOFs is crucial in force-field-based simulations of molecular adsorption in these materials,[47] and in this context it is of course desirable that these charges correctly reproduce the electrostatic potential in the MOF's pores. We chose materials for which NACs have been previously reported. Ramsahye et al. reported ESP charges from a nonperiodic cluster model of the MOF large-pore MIL-53 (Al) and Mulliken charges for the periodic crystal.[48] The c1 and c2 reference densities gave approximately equal NACs for this material. Figure 2 shows the structure of this MOF and compares the Bader and DDEC/c1 NACs to the previous results. The ESP and DDEC/c1 NACs were approximately the same. The Mulliken (Bader) NACs were strongly correlated to the DDEC/c1 NACs but had significantly lower (higher) magnitudes. Table 5 lists the ΔV_{NAC} and ΔV_{dip} values for several different charge methods applied to this MOF. Due to the effects of capping atoms in the nonperiodic cluster model, using Ramsahye et al.'s ESP results for the periodic unit cell gives a system whose NACs do not sum to zero; therefore, ΔV_{NAC} for these charges is arbitrarily large, illustrating the advantage of assigning charges in systems like this using the fully periodic system

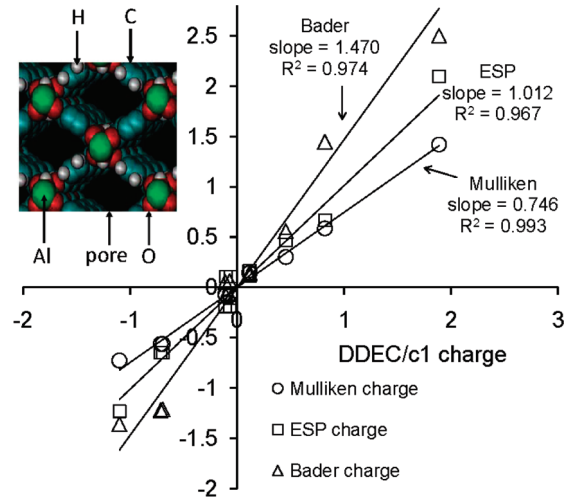

Figure 2. A comparison of ESP, Bader, and Mulliken atomic charges to the DDEC/c1 charges for the MOF MIL-53 (Al).

Table 5. Charge Analysis for Large-Pore MIL-53 (Al), with Methods Listed in Order of Ability to Reproduce *V*

Atom	ISA	DDEC c1(c2)	UC	HD	IH	no charges	Mulliken[48]	Bader	ESP for fragment[48]
ΔV_{NAC}	2.3	2.9 (2.6)	3.0	3.0	4.8	4.9	5.1	14.3	n.a.
ΔV_{dip}	0.9	1.2 (1.2)	1.2	3.2	3.1		n.a.	n.a.	n.a.
α	1	1.05 (1.01)	1.07	0.25	1.43		0.76	1.45	1.09
R^2	1	0.994 (0.997)	0.997	0.977	0.984		0.985	0.965	0.970

Table 6. Charge Analysis for IRMOF-1, with Methods Listed in Order of Ability to Reproduce *V*

atom	REPEAT method[8]	ISA	ESP for fragment[49]	UC	DDEC c1(c2)	ESP for fragment[50]	HD	no charges	Bader
Zn	1.28	1.27	1.26	1.32	1.21 (1.16)	1.31	0.42		1.30
O_1	−1.57	−1.59	−1.44	−1.68	−1.40 (−1.33)	−1.79	−0.34		−1.23
O_2	−0.61	−0.66	−0.67	−0.68	−0.66 (−0.62)	−0.63	−0.22		−1.13
C_1	0.52	0.73	0.68	0.79	0.76 (0.69)	0.62	0.18		1.37
C_2	0.14	−0.08	0.06	−0.16	−0.15 (−0.12)	0.05	−0.01		0.11
C_3	−0.18	−0.10	−0.16	−0.05	−0.06 (−0.06)	−0.12	−0.02		0.22
H	0.17	0.15	0.16	0.12	0.12 (0.12)	0.12	0.04		−0.16
ΔV_{NAC}	0.7	1.0	1.4	1.4	1.5 (1.3)	1.7	2.7	4.2	23.6
ΔV_{dip}	n.a.	0.7	n.a.	0.9	0.9 (0.9)	n.a.	4.0		n.a.
α	1	1.02	0.97	1.07	0.94 (0.90)	1.09	0.27		1.03
R^2	1	0.981	0.989	0.969	0.960 (0.967)	0.993	0.946		0.785

rather than a nonperiodic cluster. ΔV_{NAC} for the remaining methods followed the trend: ISA < DDEC < UC < HD < IH < no charges < Mulliken < Bader. For the ISA, DDEC, UC, and IH methods, ΔV_{dip} was less than ΔV_{NAC}, and the inclusion of atomic dipoles improves the accuracy of the force field for this material. NACs for different charge methods were fit to a line of the form $q = \alpha q_{best}$, where q_{best} was the set of NACs that most accurately reproduced *V* (i.e., the ISA charges). The DDEC, UC, and ESP for fragment methods had slopes and correlation coefficients (R^2) very close to 1, indicating that they give charges similar to the optimal values. On the other hand, the HD, IH, Mulliken, and Bader methods have slopes or correlation coefficients significantly different from 1, indicating that they do not give charges similar to the optimal values.

The recently developed REPEAT method provides electrostatic potential derived atomic charges using a modified error functional that eliminates the need to build a nonperiodic cluster model to obtain *V*-fit NACs for porous periodic systems.[8] Table 6 compares the NAC, ΔV_{NAC}, and ΔV_{dip} values of IRMOF-1 (also called MOF-5) for several AIM methods to those of the REPEAT method and those determined using the ESP method applied to two different nonperiodic clusters. In Table 6, the unique atoms are labeled according to Figure 6b of Campana et al.[8] ΔV_{NAC} for these methods followed the trend REPEAT < ISA < ESP fragment 1, UC, DDEC < ESP fragment 2 < HD < no charges < Bader. (The IH method failed, because it tried to assign a charge magnitude >3 for some of the oxygen atoms.) Thus, the REPEAT method was the most accurate for obtaining force-field charges in this porous periodic system. This implementation of the REPEAT method did not involve any constraints and thus would not be applicable to systems with buried atoms. Of the methods directly applicable to systems with buried atoms, the DDEC and UC methods were the most accurate at reproducing *V*. NACs for different charge methods were fit to a line of the form $q = \alpha q_{best}$, where q_{best} was the set of NACs that most accurately reproduced *V* (i.e., the REPEAT charges). The ISA, DDEC, UC, and ESP for fragment methods had slopes and correlation coefficients (R^2) close to 1, indicating that they give charges similar to the optimal values. The c1 and c2 reference densities gave similar results. On the other hand, the HD and Bader methods had slopes or correlation coefficients significantly different from 1, indicating that they do not give charges similar to the optimal values.

As an example of applying our methods to a large molecular system including heavy atoms, we studied the reaction of Stanciu et al.,[51] in which a 129-atom Zr complex with two bulky bidentate ligands reacts with two O_2 molecules to form a bisperoxy complex. It is important in examples of this kind to characterize charge transfer within the complex before and after reaction. The reaction scheme and contour surfaces for a density value of 0.1 are shown in Figure 3. These contour surfaces show that the charge density concentrates into regions surrounding each ligand, each O_2 molecule, and the metal. Table 7 summarizes the net charges of atoms in these regions computed using several different charge methods. NPA, Bader, DDEC, and UC give similar results and show a charge of ∼+2 residing on the Zr both before and after oxidation. These four methods show that a charge of ∼−1.2 is transferred from each ligand to each O_2

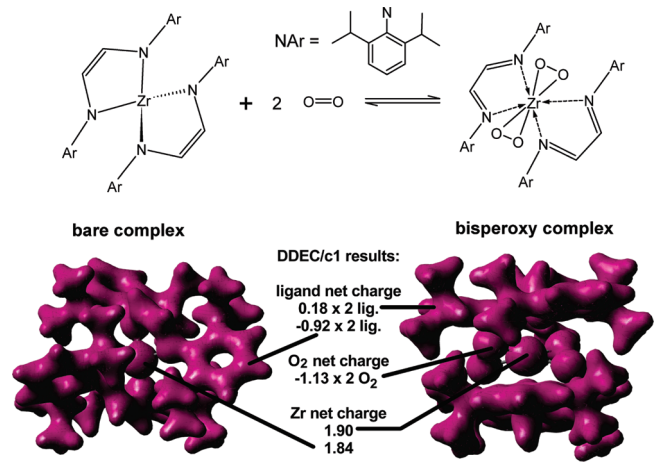

Figure 3. Charge analysis for an electron transfer reaction.

Table 7. Charges for Components of the Zr Complex of Figure 3 after and before Oxidation

	bisperoxy complex			bare complex	
	Zr	O_2	ligand	Zr	ligand
Bader	2.36	−1.24	0.06	2.20	−1.10
DDEC/c1	1.90	−1.13	0.18	1.84	−0.92
DDEC/c2	1.90	−1.09	0.14	1.96	−0.98
HD	0.74	−0.59	0.22	0.84	−0.42
IH	2.60	−1.27	−0.03	2.64	−1.32
ISA	1.66	−0.99	0.16	1.40	−0.70
Mulliken	1.20	−0.90	0.30	1.51	−0.65
NPA	2.00	−1.21	0.21	1.92	−0.96
UC	2.04	−1.13	0.11	2.10	−1.05

during oxidation. The HD, ISA, and Mulliken methods gave lower charge magnitudes, while the IH method gave higher charge magnitudes.

We now consider the accurate characterization of molecular multipoles for gas-phase molecules. Because V at large distances from a molecule is dominated by the lowest-order nonzero molecular multipole moment (MMM), atomistic simulations of gas-phase molecules should use force fields that accurately reproduce the leading MMM. Using formamide ($CHONH_2$) as an example, the molecular dipole magnitude (μ) from each method discussed above was compared to μ defined from the full electron density on the grid density used in the calculation of the NACs. As shown in Table 8, NACs from six of the methods gave small errors in μ: −0.01 (ESP), 0.02 (DDEC and UC), 0.03 (ISA), 0.09 (Mulliken), and 0.11 (IH). The remaining methods gave much larger μ errors: 0.34 (NPA), −0.43 (HD), and 0.84 (Bader). The molecular dipole vector is the sum of the dipole vector due to the NACs and the atomic dipole vectors, so AIM methods that give small atomic dipole magnitudes also give NACs that accurately reproduce μ. As noted above, including F_{ESP} in eq 8 makes the atomic dipole magnitudes small. This means DDEC, ISA, and UC will give more accurate molecular dipoles than other AIM methods for most molecules, not just formamide. For formamide, ΔV_{NAC} followed the trend ESP < ISA < UC, DDEC < IH < Mulliken < NPA < HD < Bader < no charges. ΔV_{NAC} for the best four methods (ESP, ISA, UC, and DDEC) differed by only 0.3 kcal/mol. The RMS difference between the DDEC/c1 and ESP NACs was 0.06e, which was greater than that for the ISA method (0.02), but less than that for the IH (0.07), NPA (0.09), Bader (0.35), Mulliken (0.37), and HD (0.43) methods. Similar NACs, dipole moments, and ΔV_{NAC} were obtained for the c1 and c2 reference densities. Repeating the DDEC/c1 calculation on $\rho(\vec{r})$ obtained from a DFT calculation using plane-waves instead of 6-311++G** basis sets gave only a 0.01e RMS change in NACs, which shows that the DDEC NACs are insensitive to the basis sets used to generate the electron density if the basis set size is adequate.

A useful feature of the DDEC approach is that the DDEC AMs are the multipole moments of $\rho_A^{val}(\vec{r}_A)$, because the core density for each atom does not contribute to the AMs by symmetry. The pth order MMM can be directly formed from the AMs up to order p.[20,21] Therefore, including up to pth order DDEC AMs in the force field exactly reproduces the molecular multipole moments of the valence density up to order p. Due to the finite grid spacing used in DDEC computation, these MMMs may differ by a small amount from those of the full wave function, but this can of course be reduced to an arbitrary level by refining the grid. A key drawback of the ESP method is that adding atomic dipoles requires a new optimization, which leads to new atomic charges. For example, the N charge in formamide changed from −0.89 to −1.47 when atomic dipoles were added to the ESP method; moreover, the atomic dipoles were large in magnitude ($AM_{max} = 1.5$). The DDEC method does not have this drawback, as the atomic charges are unchanged regardless of the number of AMs used and the AMs are optimized to be small in magnitude. For formamide, including atomic dipoles decreased the DDEC/c1 RMS V error from 1.6 to 1.1 kcal/mol and increased the ESP RMS V error from 1.3 to 11.8 kcal/mol. The increase in RMS V error when atomic dipoles are added to the ESP method is possible because the grid points used to evaluate the force field's RMS V error were not the same as those used to fit the atomic dipoles. The poor performance of the ESP method when atomic dipoles are included is due to the large AM_{max}. The DDEC approach does not have this problem and provides a useful framework for defining AMs in situations where extremely accurate approximation of the electrostatic potential outside the electron distribution is desired.

Finally, we consider the formal relationship between the DDEC method and computational chemistry methods. Like DFT, the DDEC method assumes electron transfer occurs

Table 8. Charge Analysis for Formamide, with Methods Listed in Order of Ability to Reproduce V

	net atomic charges						quantitative measures of V fitting			
	C	O	N	H[b]	H[c]	H[c]	$\Delta\mu$[a]	ΔV_{NAC}	ΔV_{dip}	AM_{max}
ESP	0.62	−0.53	−0.89	−0.01	0.42	0.38	−0.01	1.3	n.a.	n.a.
ISA	0.63	−0.53	−0.87	−0.01	0.40	0.38	0.03	1.4	1.0	0.4 (q)
DDEC/c2	0.58	−0.52	−0.79	0.00	0.37	0.36	0.02	1.5	1.0	0.4 (q)
UC	0.62	−0.54	−0.82	0.00	0.38	0.37	0.02	1.5	1.0	0.4 (q)
DDEC/c1	0.59	−0.53	−0.76	0.00	0.36	0.35	0.02	1.6	1.1	0.5 (q)
IH	0.50	−0.47	−0.81	0.04	0.37	0.36	0.11	2.1	2.3	0.9 (q)
Mulliken	0.00	−0.33	−0.29	0.09	0.27	0.25	0.09	3.9	n.a.	n.a.
NPA	0.47	−0.57	−0.79	0.10	0.40	0.39	0.34	4.3	n.a.	n.a.
HD	0.09	−0.28	−0.12	0.04	0.13	0.13	−0.43	5.4	1.9	1.0 (q)
Bader	1.27	−1.02	−1.12	0.04	0.43	0.40	0.84	12.5	4.9	2.9 (q)
ESP + dipoles	0.92	−1.00	−1.47	0.33	0.80	0.41	0.00	14.6	11.8	1.5 (d)
no charges							−1.56	16.2	n.a.	n.a.

[a] Error in μ compared to grid electron density. [b] H bonded to C. [c] H bonded to N.

Table 9. Charge Analysis for Formamide and Three Ozone States Using Different Exchange-Correlation Theories

				ISA		DDEC/c1		DDEC/c2	
	μ (au)	X−O (Å)	O−O−O (deg)	μ_{NAC}	q_O[a]	μ_{NAC}	q_O[a]	μ_{NAC}	q_O[a]
formamide ($q_O = -0.56 \pm 0.03$, $\mu_{NAC} = 1.60 \pm 0.02$)									
PW91	1.56	1.22		1.58	−0.53	1.58	−0.53	1.58	−0.52
B3LYP	1.59	1.21		1.63	−0.59	1.62	−0.57	1.62	−0.56
CCSD	1.54	1.21		1.62	−0.60	1.61	−0.59	1.60	−0.58
exp.	1.46[b]	1.24[b]							
ozone singlet ($q_O = 0.36 \pm 0.03$, $\mu_{NAC} = 0.45 \pm 0.03$)									
PW91	0.25	1.28	118.4	0.46	0.37	0.46	0.37	0.45	0.36
B3LYP	0.27	1.26	118.5	0.48	0.40	0.49	0.40	0.47	0.39
CCSD	0.25	1.24	117.8	0.46	0.37	0.46	0.38	0.45	0.37
CAS(12,9)	0.21	1.28	116.9	0.40	0.32	0.41	0.32	0.40	0.31
exp.	0.21[c]	1.27[d]	116.8[d]						
ozone triplet ($q_O = 0.21 \pm 0.03$, $\mu_{NAC} = 0.34 \pm 0.06$)									
PW91	0.29	1.35	99.3	0.35	0.21	0.34	0.21	0.33	0.20
B3LYP	0.32	1.32	99.2	0.38	0.23	0.37	0.23	0.37	0.22
CCSD	0.32	1.32	97.5	0.39	0.24	0.39	0.23	0.38	0.23
CAS(12,9)	0.22	1.36	99.3	0.21	0.16	0.26	0.16	0.26	0.16
exp.		1.35[e]	98.9[e]						
ozone +1 doublet ($q_O = 0.48 \pm 0.05$, $\mu_{NAC} = 0.14 \pm 0.03$)									
PW91	0.01	1.23	134.3	0.14	0.49	0.14	0.49	0.14	0.48
B3LYP	0.01	1.21	134.6	0.18	0.54	0.18	0.54	0.17	0.53
CCSD	0.01	1.18	133.4	0.14	0.50	0.15	0.50	0.14	0.49
CAS(11,9)	0.04	1.23	128.1	0.09	0.42	0.09	0.42	0.08	0.41
exp.		1.25[f]	131.5[f]						

[a] For ozone, the center O atom has charge q_O, and each outer O atom has charge $-q_O/2$ (singlet, triplet) or $(1 - q_O)/2$(+1 cation). [b] Ref 54. [c] Ref 55. [d] Ref 56. [e] Ref 57. [f] Ref 53.

to minimize a system's energy subject to optional constraints; therefore, the DDEC method is applicable to the same types of systems as DFT. Optional constraints include fixing the net charge, one or more atomic positions, and the number of up electrons minus down electrons. As described above, the DDEC charge distributions depend only on $\rho(\vec{r})$, the reference densities, and χ. Quantum chemistry methods such as DFT, coupled cluster theory, configuration interaction, and quantum Monte Carlo can formally reproduce the exact $\rho(\vec{r})$ in the limit of an exact exchange-correlation methodology with relativistic corrections and arbitrarily large basis sets. All these methods yield the same $\rho(\vec{r})$ and thus identical DDEC charges in this limit. Actual computations involve compromises that approximate $\rho(\vec{r})$, and this causes different computational chemistry methods to give slightly different DDEC charges.

A system is called single-reference if the configuration interaction expansion of its wave function has one Slater determinant whose coefficient is an order of magnitude greater than that of any other Slater determinant; otherwise, the system is called multireference. Examples in this article are single-reference systems, except for the magnetic systems (Fe_2O_3, Fe_2SiO_4, and Fe_3O_4) discussed above and the ozone states discussed below. (Ozone is a commonly studied multireference system.[52,53]) In antiferromagnetic systems like Fe_2O_3 and Fe_2SiO_4, each magnetic center (e.g., Fe atom) has a quantum superposition of spin-up and spin-down magnetism. When applying DFT to these antiferromagnetic systems, we used the common technique of breaking symmetry by assigning spin-up magnetism to one Fe atom and spin-down magnetism to the other Fe atom in the unit cell, and this approximation gave reasonable $\rho(\vec{r})$ and NACs. For small systems, the complete active space (CAS) and related methods can be used to find correlated multireference wave functions.

Table 9 shows dipole moments, select geometric parameters, and oxygen charges for formamide and three ozone states using different exchange-correlation theories. μ and μ_{NAC} are the dipole moments due to $\rho(\vec{r})$ and the NACs, respectively. AUG-cc-pVTZ basis sets were used for coupled-cluster theory with single and double excitations (CCSD) and CAS, and 6-311++G** basis sets were used for the DFT methods. CAS(n,m) denotes an active space containing n electrons and m orbitals. $m = 9$ and $n = 12$ (11 for +1 cation) are the same size as the 2p valence space for 3 O atoms and a reasonable choice for the active space. In the CAS calculations, molecular orbitals with the lowest energy eigenvalues were fully occupied, those with the highest eigenvalues were completely unoccupied, and those with intermediate eigenvalues were included in the active space. The ozone potential energy surface contains dozens of equilibrium geometries having various spin multiplicities and net charges.[52,53] Here, we consider three equilibrium structures that are similar to the experimentally observed global energy minima for the singlet, triplet, and +1 doublet states. Each of these structures has two equal O−O bond lengths. The similarity of the computed and experimental geometries verifies that the appropriate minima on the potential energy surface have been found. For each state, the average and standard deviation of q_O and μ_{NAC} are given in parentheses in Table 9. Each average and standard deviation included all the levels of theory (PW91, B3LYP, CCSD, and CAS for ozone states) and charge methods (ISA, DDEC/c1, and DDEC/c2). In each case, the standard deviation was small (≤ 0.06), because different levels of theory and charge

methods gave similar results. Most importantly, the standard deviation for a given molecular state was much smaller than the change observed between two different molecular states. For example, $q_O = 0.21 \pm 0.03$ for the ozone triplet state was decisively lower than $q_O = 0.36 \pm 0.03$ for the ozone singlet state. For a given molecular state, the maximum change in q_O between two different exchange-correlation theories was 0.13 even when changing between c1 and c2 reference densities. The overall message from Table 9 is that DDEC charges can be reliably computed for a variety of computational chemistry methods, including DFT, coupled-cluster theory, and multireference methods like CAS.

Additional tests showed that the DDEC NACs depend less on the exchange-correlation theory used to compute the reference densities than they do on the exchange-correlation theory used to compute $\rho(\vec{r})$. For the five bulk materials in Table 3, the RMS change in NAC (Δq_{rms}) for c1 ref densities computed with the Ceperley-Alder LSDA functional versus PW91 (geometry and $\rho(\vec{r})$ from LSDA in both cases) was $0.023e$. This was smaller than $\Delta q_{rms} = 0.026e$ when the geometry and $\rho(\vec{r})$ were obtained from LSDA versus PW91 (using PW91 c1 ref densities in both cases). When the geometries, $\rho(\vec{r})$, and c1 ref densities were all computed with LSDA versus PW91, the change was slightly larger ($\Delta q_{rms} = 0.031e$). For the three magnetic materials in Table 4, $\Delta q_{rms} = 0.034e$ when the c1 ref densities were recomputed with PBE. Similar insensitivity was also observed for the c2 ref densities. Specifically, for the four BN structures in Table 2, $\Delta q_{rms} = 0.006e$ when the c2 ref densities were recomputed with the hybrid functional MPW1PW91. For formamide using PW91 c2 ref densities, $\Delta q_{rms} = 0.037$ $(0.059)e$ for geometry and $\rho(\vec{r})$ from B3LYP (CCSD) versus PW1. When c2 ref densities were recomputed with MPW1PW91, all of the B3LYP, CCSD, and PW91 NACs for formamide changed by less than $0.005e$. These results show it is not necessary to compute the reference densities and $\rho(\vec{r})$ with the same exchange-correlation theory. The optimal exchange-correlation functional for computing the reference densities should correctly reproduce each element's ground state electron configuration. The PW91 functional did this for all of the elements we studied, so all of the NACs given in Tables 1−9 used PW91 reference densities.

Conclusions

A systematic comparison has been made between different methods for computing atomic charges, with particular emphasis on AIM methods. Although a unique definition for the charge associated with an atom in a material does not exist, we believe an ideal AIM method should satisfy several criteria. First, it should give NACs that reflect the amount of charge transfer between atoms. For example, it should give NACs that are approximately less than or equal to the formal oxidation state for ionic compounds. Second, it should give NACs that approximately reproduce V outside the electron distribution. Third, it should be applicable to a wide variety of materials, including periodic and nonperiodic materials with and without buried atoms. Fourth, it should give NACs with good transferability between closely related systems. We provided evidence that existing AIM methods fall short of these goals. Prior research has shown that the HD method almost always underestimates NACs,[10,11] and our results confirm this. Upon calculating IH and ISA NACs for the first time in periodic materials, we found that these methods do not work well for nonporous solids. The ISA method is problematic for systems containing buried atoms, while the IH method overestimates charge magnitudes in many extended systems. Because the ISA method does not require the calculation of reference densities, it is an appealing method for calculating NACs in systems that do not contain buried atoms, and we found that it accurately reproduced V in these systems. The Bader method consistently gave chemically reasonable charges for the nonporous solids we studied, but Bader NACs did not accurately reproduce V outside the electron distribution in porous materials.

We developed a new AIM method, called density derived electrostatic and chemical (DDEC) charges to address these problems. DDEC optimizes the NACs to be chemically meaningful and to reproduce V outside the electron distribution by simultaneously optimizing atomic electron density distributions to be close to spherically symmetric and to resemble reference state atoms. For accurate calculation of atomic charges in extended systems, we found that the reference densities must include the effects of charge compensation. These improvements allow the DDEC method to account for three different types of charge transfer that take place in materials: (a) ionic bonding, (b) covalent bonding, and (c) charge compensation and dielectric screening. Charge analysis was performed for a B_4N_4 cluster, a hexagonal BN sheet, a BN nanotube, nine nonporous solids (h-BN, NaF, NaCl, MgO, MgH_2, $SrTiO_3$, Fe_2O_3, Fe_2SiO_4, and Fe_3O_4), a NaF slab, a $SrTiO_3$ slab, the MIL-53 (Al) MOF, IRMOF-1, a $ZrN_4C_{52}H_{72}$ organometallic complex, a $ZrO_4N_4C_{52}H_{72}$ organometallic complex, formamide, and three ozone states (singlet, triplet, and +1 cation). These examples included systems with periodicity along zero, one, two, and three dimensions; porous and nonporous solids; solid surfaces; and both large and small molecules. The DDEC method consistently gave reasonable charges in a wide variety of periodic and nonperiodic materials with and without buried atoms. The DDEC NACs were consistent with experimental results for NaF, MgO, $SrTiO_3$, and a series of oxides containing iron, and for these systems showed slightly better correspondence than the Bader charges to the experimental data. Furthermore, the DDEC NACs were not sensitive to the basis sets used to generate the electron density. However, the DDEC method often overestimated charge magnitudes by a few hundredths of a unit for completely ionic solids.

Two methods were developed for calculating charge compensated reference densities. In the c1 method, each ion is placed in the center of a 10 Å × 10 Å × 10 Å periodic unit cell made neutral by a uniform background charge. The c2 method does not involve periodicity and places each ion in the center of a spherical shell of compensating charge. For anions, the compensating charge is chosen to make the electric field zero infinitesimally outside the shell radius which is varied to minimize the system's total energy. These

optimized radii were similar to crystal-structure-derived anionic radii from the literature (where available). For a $+q$ cation, the compensating charge is constrained to $-q$ and the shell radius is set equal to the average radius of the outermost q occupied Kohn−Sham spin−orbitals in the neutral atom. The DDEC/c1 and DDEC/c2 methods gave similar results for all of the systems we studied. The c1 and c2 reference densities computed with the PW91 functional gave good performance even when $\rho(\vec{r})$ for the system being studied was computed with a different level of theory (e.g., PBE, B3LYP, LSDA, CCSD, or CAS); thus, it is not critical to recompute the reference densities at different levels of theory. Between different reference density sets or exchange-correlation theories, the DDEC NACs usually differed by $\leq 0.1e$. The DDEC NACs were also within $0.1e$ of experimental charges for NaF and MgO. All of these results suggest that the DDEC NACs can be routinely computed with an absolute accuracy of approximately $0.1e$.

Tests were performed to assess the relative ability of NACs computed using different methods to reproduce V outside the electron distribution. The ESP method, and its recent extension to periodic materials called the REPEAT method, were found to be the most accurate methods for reproducing V in nonperiodic and periodic materials, respectively. This is expected, because these two methods specifically optimize the NACs to minimize ΔV_{NAC}. Unlike the ESP and REPEAT methods, the DDEC method does not require the addition of constraints to handle systems with buried atoms. Of the methods we tested that were applicable to systems with buried atoms, the DDEC method was found to be the most accurate for reproducing V outside the electron distribution. The Mulliken, HD, and Bader methods were found to be inaccurate for reproducing V. Because DDEC charges are optimized to resemble a chemical reference state, they exhibited better transferability than charges simply optimized to fit V. Because the AMs are optimized to be small, DDEC NACs accurately reproduce the dipole moments of molecules and can be used to quantify the amount of charge transfer between atoms during chemical reactions. We anticipate that DDEC charges will find application in the development of interatomic potentials for atomistic simulations of complex materials, particularly for spatially periodic materials containing buried atoms.

Acknowledgment. Financial support was provided by the National Science Foundation through grant CHE0651182 and the Department of Energy through contract DE-SC0001058. Supercomputing resources were provided by Georgia Institute of Technology and Teragrid grants TG-CHE090019 and TG-CTS100027.

Supporting Information Available: Coordinates of optimized geometries, more extensive results tables, and sample input files for computing the c2 reference densities. This material is available free of charge via the Internet at http://pubs.acs.org.

References

(1) Phillpot, S. R.; Sinnott, S. B. *Science* **2009**, *325*, 1634–1635.

(2) Wiberg, K. B.; Rablen, P. R. *J. Comput. Chem.* **1993**, *14*, 1504–1518.

(3) Sigfridsson, E.; Ryde, U. *J. Comput. Chem.* **1998**, *19*, 377–395.

(4) Singh, U. C.; Kollman, P. A. *J. Comput. Chem.* **1984**, *5*, 129–145.

(5) Dognon, J.-P.; Durand, S.; Granucci, G.; Levy, B.; Millie, P.; Rabbe, C. *J. Mol. Struct.* **2000**, *507*, 17–23.

(6) Bayly, C. I.; Cieplak, P.; Cornell, W. D.; Kollman, P. A. *J. Phys. Chem.* **1993**, *97*, 10269–10280.

(7) Sherwood, P.; de Vries, A. H.; Collins, S. J.; Greatbanks, S. P.; Burton, N. A.; Vincent, M. A.; Hillier, I. H. *Faraday Disc.* **1997**, *106*, 79–92.

(8) Campana, C.; Mussard, B.; Woo, T. K. *J. Chem. Theory Comput.* **2009**, *5*, 2866–2878.

(9) Hirshfeld, F. L. *Theor. Chim. Acta* **1977**, *44*, 129–138.

(10) Bultinck, P.; Van Alsenoy, C.; Ayers, P. W.; Carbo-Dorca, R. *J. Chem. Phys.* **2007**, *126*, 144111.

(11) Davidson, E. R.; Chakravorty, S. *Theor. Chim. Acta* **1992**, *83*, 319–330.

(12) Bultinck, P.; Ayers, P. W.; Fias, S.; Tiels, K.; Van Alsenoy, C. *Chem. Phys. Lett.* **2007**, *444*, 205–208.

(13) Bultinck, P.; Cooper, D. L.; Van Neck, D. *Phys. Chem. Chem. Phys.* **2009**, *11*, 3424–3429.

(14) Lillestolen, T. C.; Wheatley, R. J. *Chem. Commun.* **2008**, 5909–5911.

(15) Lillestolen, T. C.; Wheatley, R. J. *J. Chem. Phys.* **2009**, *131*, 144101.

(16) Van Damme, S.; Bultinck, P.; Fias, S. *J. Chem. Theory Comput.* **2009**, *5*, 334–340.

(17) Bader, R. F. W.; Macdougall, P. J.; Lau, C. D. H. *J. Am. Chem. Soc.* **1984**, *106*, 1594–1605.

(18) Bader, R. F. W.; Matta, C. F. *J. Phys. Chem. A* **2004**, *108*, 8385–8394.

(19) Reed, A. E.; Weinstock, R. B.; Weinhold, F. *J. Chem. Phys.* **1985**, *83*, 735–746.

(20) Kosov, D. S.; Popelier, P. L. A. *J. Phys. Chem. A* **2000**, *104*, 7339–7345.

(21) Laidig, K. E. *J. Phys. Chem.* **1993**, *97*, 12760–12767.

(22) Freitag, M. A.; Gordon, M. S.; Jensen, J. H.; Stevens, W. J. *J. Chem. Phys.* **2000**, *112*, 7300–7306.

(23) Nalewajski, R. F.; Parr, R. G. *Proc. Nat. Sci. Acad. U.S.A.* **2000**, *97*, 8879–8882.

(24) Maslen, E. N.; Spackman, M. A. *Aust. J. Phys.* **1985**, *38*, 273–287.

(25) Leenaerts, O.; Partoens, B.; Peeters, F. M. *Appl. Phys. Lett.* **2008**, *92*, 243125.

(26) Watson, R. E. *Phys. Rev.* **1958**, *111*, 1108–1110.

(27) Zuo, J. M.; OKeeffe, M.; Rez, P.; Spence, J. C. H. *Phys. Rev. Lett.* **1997**, *78*, 4777–4780.

(28) Hafner, J. *J. Comput. Chem.* **2008**, *29*, 2044–2078.

(29) Kresse, G.; Furthmüller, J. *Phys. Rev. B* **1996**, *54*, 11169–11186.

(30) Kresse, G.; Joubert, D. *Phys. Rev. B* **1999**, *59*, 1758–1775.

(31) Frisch, M. J.; Trucks, G. W.; Schlegel, H. B.; Scuseria, G. E.; Robb, M. A.; Cheeseman, J. R.; Scalmani, G.; Barone, V.; Mennucci, B.; Petersson, G. A.; Nakasuji, H.; Caricato, M.; Li, X.; Hratchian, H. P.; Izmaylov, A. F.; Bloino, J.; Zheng, G.; Sonnenberg, J. L.; Hada, M.; Ehara, M.; Toyota, K.; Fukuda, R.; Hasegawa, J.; Ishida, M.; Nakamjima, T.; Honda, Y.; Kitao, O.; Nakai, H.; Vreven, T.; Montgomery, J. A. J.; Peralta, J. E.; Ogliaro, F.; Bearpark, M.; Heyd, J. J.; Brothers, E.; Kudin, K. N.; Staroverov, V. N.; Kobayashi, R.; Normand, J.; Raghavachari, K.; Rendell, A.; Burant, J. C.; Iyengar, S. S.; Tomasi, J.; Cossi, M.; Rega, N.; Millam, N. J.; Klene, M.; Knox, J. E.; Cross, J. B.; Bakken, V.; Adamo, C.; Jaramillo, J.; Gomperts, R.; Stratmann, R. E.; Yazyev, O.; Austin, A. J.; Cammi, R.; Pomelli, C.; Ochterski, J. W.; Martin, R. L.; Morokuma, K.; Zakrzewski, V. G.; Voth, G. A.; Salvador, P.; Dannenberg, J. J.; Dapprich, S.; Daniels, A. D.; Farkas, O.; Foresman, J. B.; Ortiz, J. V.; Ciolowski, J.; Fox, D. J. *Gaussian 09*, Revisions up to and including A.02; Gaussian, Inc.: Wallingford, CT, 2009.

(32) Loiseau, T.; Serre, C.; Huguenard, C.; Fink, G.; Taulelle, F.; Henry, M.; Bataille, T.; Ferey, G. *Chem.—Eur. J.* **2004**, *10*, 1373–1382.

(33) Wyckoff, R. W. G. *Crystal Structures*; John Wiley & Sons: New York, 1963; Vol. 1, 85−237.

(34) Li, H.; Eddaoudi, M.; O'Keeffe, M.; Yaghi, O. M. *Nature* **1999**, *402*, 276–279.

(35) Henkelman, G.; Arnaldsson, A.; Jonsson, H. *Comput. Mater. Sci.* **2006**, *36*, 354–360.

(36) Sanville, E.; Kenny, S. D.; Smith, R.; Henkelman, G. *J. Comput. Chem.* **2007**, *28*, 899–908.

(37) Tang, W.; Sanville, E.; Henkelman, G. *J. Phys. Condens. Matter* **2009**, *21*, 084204.

(38) Smith, W. *CCCP5 Newsletter* **1998**, *46*, 18–30.

(39) Manz, T. A.; Sholl, D. S. *J. Comput. Chem.* **2010**, *31*, 1528–1541.

(40) *CRC Handbook of Chemistry and Physics*; 90 ed.; Lide, D. R., Ed.; CRC Press: Baco Raton, FL, 2009; Sec. 14, pp 11−12.

(41) York, D. M.; Karplus, M. *J. Phys. Chem. A* **1999**, *103*, 11060–11079.

(42) de Castro, E. V. R.; Jorge, F. E. *J. Chem. Phys.* **1998**, *108*, 5225–5229.

(43) Su, Z. W.; Coppens, P. *Acta Crystallogr., Sect. A* **1995**, *51*, 27–32.

(44) Ikeda, T.; Kobayashi, T.; Takata, M.; Takayama, T.; Sakata, M. *Solid State Ionics* **1998**, *108*, 151–157.

(45) Jauch, W.; Reehuis, M. *Acta Crystallogr., Sect. A* **2005**, *61*, 411–417.

(46) Yamashita, T.; Hayes, P. *Appl. Surf. Sci.* **2008**, *254*, 2441–2449.

(47) Keskin, S.; Liu, J.; Rankin, R. B.; Johnson, J. K.; Sholl, D. S. *Ind. Eng. Chem. Res.* **2009**, *48*, 2355–2371.

(48) Ramsahye, N. A.; Maurin, G.; Bourrelly, S.; Llewellyn, P.; Loiseau, T.; Ferey, G. *Phys. Chem. Chem. Phys.* **2007**, *9*, 1059–1063.

(49) Amirjalayer, S.; Tafipolsky, M.; Schmid, R. *Angew. Chem., Int. Ed.* **2007**, *46*, 463–466.

(50) Sagara, T.; Klassen, J.; Ganz, E. *J. Chem. Phys.* **2004**, *121*, 12543–12547.

(51) Stanciu, C.; Jones, M. E.; Fanwick, P. E.; Abu-Omar, M. M. *J. Am. Chem. Soc.* **2007**, *129*, 12400–12401.

(52) Kalemos, A.; Mavridis, A. *J. Chem. Phys.* **2008**, *129*, 054312.

(53) Willitsch, S.; Innocenti, F.; Dyke, J. M.; Merkt, F. *J. Chem. Phys.* **2005**, *122*, 024311.

(54) Kurland, R. J.; Wilson, E. B. *J. Chem. Phys.* **1957**, *27*, 585–590.

(55) Mack, K. M.; Muenter, J. S. *J. Chem. Phys.* **1977**, *66*, 5278–5283.

(56) Tyuterev, V. G.; Tashkun, S.; Jensen, P.; Barbe, A.; Cours, T. *J. Mol. Spectrosc.* **1999**, *198*, 57–76.

(57) Bouvier, A. J.; Inard, D.; Veyret, V.; Bussery, B.; Bacis, R.; Churassy, S.; Brion, J.; Malicet, J.; Judge, R. H. *J. Mol. Spectrosc.* **1998**, *190*, 189–197.

CT100125X